Contactless prompt tumbling-rebound of drops from a sublimating slope

Carlo Antonini[1,b], Stefan Jung[1], Andreas Wetzel[1], Emmanuel Heer[1], Philippe Schoch[1], Ali Mazloomi M.[2], Shyam S. Chikatamarla[2], Ilya Karlin[2], Marco Marengo[3] and Dimos Poulikakos[1,*]

[1] Laboratory of Thermodynamics in Emerging Technologies, Mechanical and Process Engineering Department, ETH Zurich, 8092 Zürich, Switzerland

[2] Aerothermochemistry and Combustion Systems Lab, Mechanical and Process Engineering Department, ETH Zurich, 8092 Zurich, Switzerland

[3] School of Computing, Engineering and Mathematics, University of Brighton, Lewes Road, Brighton BN2 4GJ, UK

* corresponding author: dpoulikakos@ethz.ch

[b] current address: EMPA, Swiss Federal Laboratories for Materials Science and Technology, Überlandstrasse 129, CH-8600 Dübendorf, Switzerland.

ABSTRACT

We have uncovered a drop rebound regime, characteristic of highly viscous liquids impacting onto tilted sublimating surfaces. Here the drops rather than showing a "slide, spread, recoil and rebound" behavior, exhibit a "prompt tumbling-rebound". As a result, glycerol surprisingly rebounds faster than three orders of magnitude less viscous water. When a viscous drop impacts on a sublimating surface, part of its initial linear momentum is converted into angular momentum: Lattice Boltzmann simulations confirmed that tumbling owes its appearance to the rapid transition of the internal angular velocity prior to rebound to a constant value, as in a tumbling solid body.

I INTRODUCTION

Despite its illusory simplicity, the interaction between a liquid drop and a solid surface during impact is a fascinating fluidics problem, combining a variety of phenomena at multiple temporal and spatial scales [1–5]. These include splash [6–10], phase-change induced surface levitation [11–15], skating on a film of trapped air [16–18] and rebounding [19–22]. Recently [11], it was demonstrated that drops can rebound after impact on an extremely cold solid carbon dioxide surface (at -79°C, well below the limit of even homogeneous nucleation of water), because of the formation of a sublimated vapor layer acting both as impact cushion and thermal insulator, enabling drops to hover and rebound without freezing. A sublimating surface is different from aerodynamically assisted surface levitation [23–25] and from the Leidenfrost effect [12–14,26–28], in the sense that it is independent from liquid properties, such as boiling temperature, and there is no loss of drop mass due to its own boiling (as in the Leidenfrost phenomenon). Of course, in both cases an intervening layer is generated between the drop and the substrate. Sublimating surfaces can thus be used to study the contactless interaction of virtually any liquid, such as the highly viscous liquids used here. Also, they enable the study of phenomena expected from a superhydrophobic surface (SHS) with extreme performance [29] (very high contact angles and very low hysteresis), providing further motivation for the fabrication and subsequent study of such surfaces. In the present fundamental study, we demonstrate and explain the existence of a new "prompt tumbling-rebound" mechanism, in

which a small conversion of translational to rotational kinetic energy, at non-axisymmetric impact conditions, promotes fast drop rebound despite high viscosities.

By focusing on non-axisymmetric impact conditions at increasing viscosity, we observe a transition from an expected "slide, spread, recoil and rebound" mechanism (see Figure 1a and b, and Video 1 in the Supplemental Material) to a "tumbling" behavior, enabling the prompt rebound of highly viscous liquids such as glycerol (see Figure 1c and Videos 2 and 3 in the Supplemental Material). Here, after an initial, viscosity-limited and impact-driven deformation phase, the drops simply tumble off the surface, rebounding faster than three orders of magnitude less viscous (water) drops. As confirmed by 3D numerical simulations based on the entropic lattice Boltzmann method (ELBM, see Video 4 in the Supplemental Material), the behavior at high viscosities is aided by the contactless nature of the impact and was not observed on classical superhydrophobic surfaces, where an increase of viscosity can protract the rebound time [30], or even prevent rebound. In experiments on micropillar-based tilted surfaces, we observed that viscous drops stay initially pinned at the impact point and eventually roll down the surface at a speed of approximately 10^{-2} m/s (see section SM1 for details on superhydrophobic surface preparation and Video 5 in the Supplemental Material showing viscous drop behavior). In addition, drop pinning may occur on textured superhydrophobic surfaces as a result of drop impalement at high impact speed [22,30,31]: impalement is not an issue sublimating surfaces.

A representative schematic of a plausible scenario of contactless drop impact on a tilted sublimating surface is shown in Figure 1a: after impact, the drop slides down the slope, and simultaneously spreads. The presence of the CO_2 vapor layer due to substrate sublimation significantly reduces friction between the drop and the solid substrate, playing a similar role as that of the lubricating melted liquid water layer in ice skating [32]. The drop subsequently bounces off the surface after a certain rebound time, t_{reb}, defined as the time lag the impact and the lift-off. The corresponding downhill distance travelled by the drop, L_{slide}, was measured from the impact point to the lift-off point (see Figure 1b).

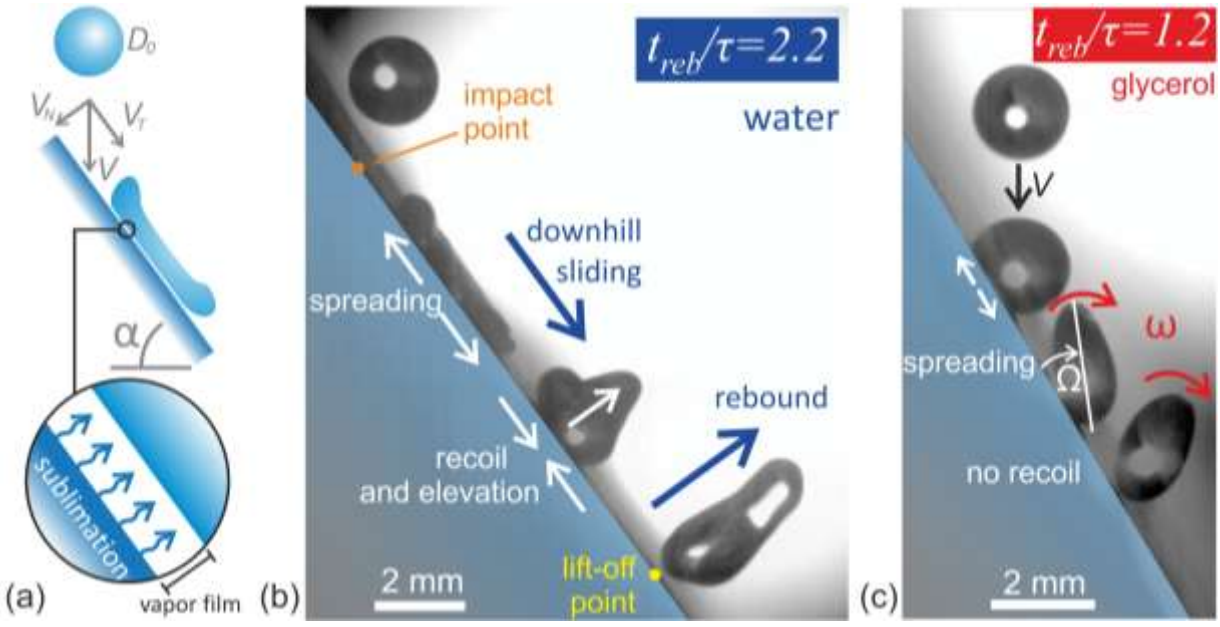

Figure 1: Drop impact onto a tilted carbon dioxide sublimating surface: schematic (a) and image sequence of water (b) and glycerol (c) drop impacts. Impact conditions are: $\alpha = 55^o$, $We = \rho V^2 D_0/\sigma = 86$, $Oh = \mu/\sqrt{\rho\sigma D_0} = 2.7\cdot 10^{-3}$ for water, and $\alpha = 60^o$, $We = 121$, $Oh = 3.2$ for glycerol. Image sequence was obtained by overlapping of 4 images: see Video 1 and 2 in the Supplemental Material for full sequence. The non-dimensional rebound time is $t_{reb}/\tau = 2.2$ for water, and $t_{reb}/\tau = 1.2$ for glycerol. Also indicated are the normal, V_N, and tangential, V_T, components of impact velocity, as well as the substrate tilt angle, α.

II METHODS AND MATERIALS

A Experimental tests

Drop impact studies were performed at room temperature (T≈23°C) on a carbon dioxide disk at -79°C, corresponding to the CO_2 sublimation temperature at 1 atm. The surface was first kept horizontal to study normal impacts as a basis for comparison, and was subsequently tilted up to an angle of 75° to study oblique impacts. Most of the experiments were conducted using water, glycerol, and water-glycerol mixtures, spanning over three orders of magnitude of viscosity (from ~1 to ~10^3 mPas), and surface tension $63 < \sigma < 72$ mN/m. Additional normal impact experiments were performed with glycols and silicon oils, with surface tension down to 20 mN/m (see details in section SM2 in the Supplemental Material). The drop impact velocities and drop diameters were $0.8 < V < 3.2$ m/s and $1.3 < D_0 < 2.1$mm, respectively. The

corresponding non-dimensional number ranges were for the Weber number, $20 < We = \rho V^2 D_0 / \sigma < 610$, for the Reynolds number, $1.45 < Re = \rho V D_0 / \mu < 5490$, and for the Ohnesorge number, $2.7 \cdot 10^{-3} < Oh = \mu / \sqrt{\rho \sigma D_0} < 4.92$.

B Numerical simulations

To provide insight for the appearance of tumbling, we used the ELBM modeling approach [33], employing the Navier-Stokes equations for a two-phase fluid, where a van der Waals-type equation of state and Korteweg's stresses are implemented in the kinetic lattice Boltzmann setting of discrete velocity populations [34–36]. The impacting liquid was modeled as a drop on a superhydrophobic surface [37] with the contact angle $\theta = 180^\circ$ and partial slip at the wall – see Ref. [38] for details on application of boundary conditions for the lattice Boltzmann populations at the wall. Partial slip at the wall was imposed using the slip coefficient, k, obtained from the experimental measurements, presented below. The tangential velocity at the wall nodes was made equal to $kV_t^{'}$, where $V_t^{'}$ is the tangential velocity at the neighboring node within the fluid, in the direction perpendicular to wall, thus locally enforcing the partial slip observed in the experiments. This procedure helps us circumvent explicit modeling of the sub-micron gas layer trapped between the drop and the substrate. The validity of the numerical simulations is confirmed *a posteriori* from the good prediction of the rebound time, angular velocity and drop shape, in comparison to the experiments.

III RESULTS AND DISCUSSION

A Normal axisymmetric impacts

The identification of a transition in the drop dynamics at high viscosity, i.e. high Oh, can be understood by first looking at the behavior of drops during normal impact on horizontal surfaces (Figure 2) and then oblique impact on tilted surfaces (Figure 3 and Figure 4Figure 4). Figure 2a illustrates the rebound/no-rebound behavior on the $We-Oh$ plane, for normal drop impact on a horizontal sublimating substrate. It is found that a transition from rebound to no-rebound occurs at $Oh\approx 1$, with low viscosity drops always rebounding for $Oh<0.6$, and high viscosity drops unable to lift-off for $Oh>1.2$. In the in-between transition regime, either outcome is possible. The transition regime at $Oh\approx 1$ can be explained by the fact that in this range the viscous effects become of the same order as the surface energy effects, and cause a rapid dissipation of the initial kinetic energy of the impacting drop: viscous effects thus inhibit the conversion of kinetic energy into surface potential energy, and back to kinetic energy, as typically occurs for relatively low viscosity liquids, such as water, and prohibit rebound. As shown in the inset picture in Figure 2b, at high Oh the highly viscous drops bead up to a quasi-spherical shape at rest, and eventually roll away at the slightest perturbation, because of the absence of wetting and lateral adhesion forces due to the sublimating substrate. In the rebound regime, the rebound time follows the conventional scaling $t_{reb}/\tau = a = \text{const}$, where $\tau=\left(\rho D_0^3/8\sigma\right)^{0.5}$ [19] and $a=2.2\pm0.2$ [20], with a being constant and independent of the Ohnesorge number (see also more details in Section SM3 in the Supplemental material).

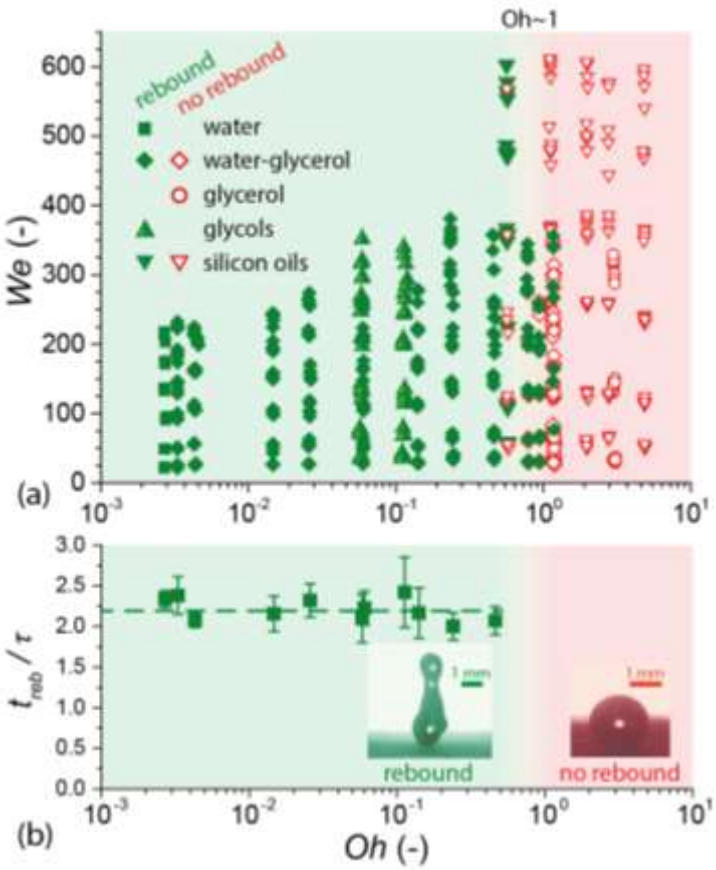

Figure 2: (a) Rebound/no rebound map for normal drop impact on a horizontal sublimating surface (603 impact tests with different liquids - see legend). (b) Non-dimensional rebound time, t_{reb}/τ, as function of the Ohnesorge number, Oh.

B Oblique non-axisymmetric impacts

For non-axisymmetric impacts on tilted sublimating surface, however, experiments reveal a qualitative change of the rebound pattern, showing that highly viscous glycerol drops can also rebound, and do this even faster than water drops. The characteristic sliding velocity of the drop, V_{slide}, computed as the ratio L_{slide}/t_{reb}, is plotted in Figure 3a as function of the tangential component of the impact velocity, V_T. In the ideal inviscid case, assuming zero lateral adhesion forces [39,40] to cause drop deceleration and negligible acceleration due to gravity, the drop will continue to travel on the substrate at $V_{slide} \approx V_T$. A linear scaling

$V_{slide} = kV_T$ holds for all tested liquids, with k depending on the Ohnesorge number (see Figure 3b). For a millimetric water drop ($Oh = 2.7 \cdot 10^{-3}$), $k = 0.9$, remarkably close to the ideal inviscid case, $k = 1$, and three-fold higher than for water drops impacting on a superhydrophobic surface ($k = 0.3$, as reported previously [17]). The enhanced sliding on a sublimating surface, even with respect to a superhydrophobic surface, is a consequence of the contactless regime, in which lateral adhesion forces are absent. The value of k decreases with increasing Ohnesorge number (see Figure 3b), and subsequently plateaus remaining approximately constant at the value of $k \approx 0.6$ for $Oh > 1$, as shown by experiments. Values of $k < 1$ denote that frictional losses in the vapor layer trapped between the drop and the substrate, despite being smaller than on superhydrophobic surfaces, are not negligible. As confirmed by the entropic lattice Boltzmann method, viscous losses occur mainly in the first (spreading) phase of the impact, over a timescale t_{fr}, as a result of the drop rapid deformation and wall friction. Thus, the friction force can be estimated as $F_{fr} \approx m\left(V_T - V_{slide}\right)/t_{fr} = mV_T(1-k)/t_{fr}$, which we will use below to estimate the drop angular velocity during tumbling. A thorough understanding of the dependence of k on the Ohnesorge number, beyond the clear trend shown by the experimental data, would require the accurate reconstruction of the vapor layer flow at the liquid-solid interface through numerical simulations, a challenge that goes beyond the goals of the present study, and can certainly represent a motivation for future works.

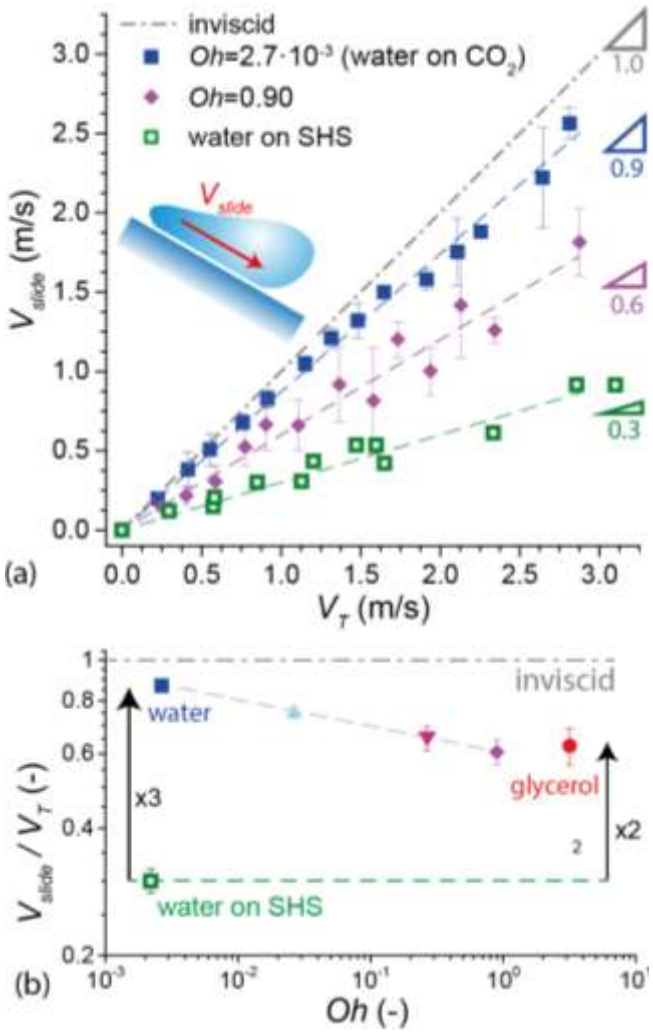

159

160 **Figure 3:** (a) Drop average sliding velocity, V_{slide}, as function of impact tangential velocity, V_T. V_{slide} is calculated as
161 the ratio L_{slide}/t_{reb}. Legend reports values of the corresponding non-dimensional Ohnesorge number, Oh. (b) Ratio
162 $k = V_{slide}/V_T$ as function of Oh. Symbol legend: experimental data for impacts on the sublimating substrate (■
163 water, ▲ water/glycerol 40/60, ▼ water/glycerol 15/85, ♦ water/glycerol 7/93, ● glycerol); □ water drop impact on a
164 superhydrophobic surface (SHS, data from [41]).
165

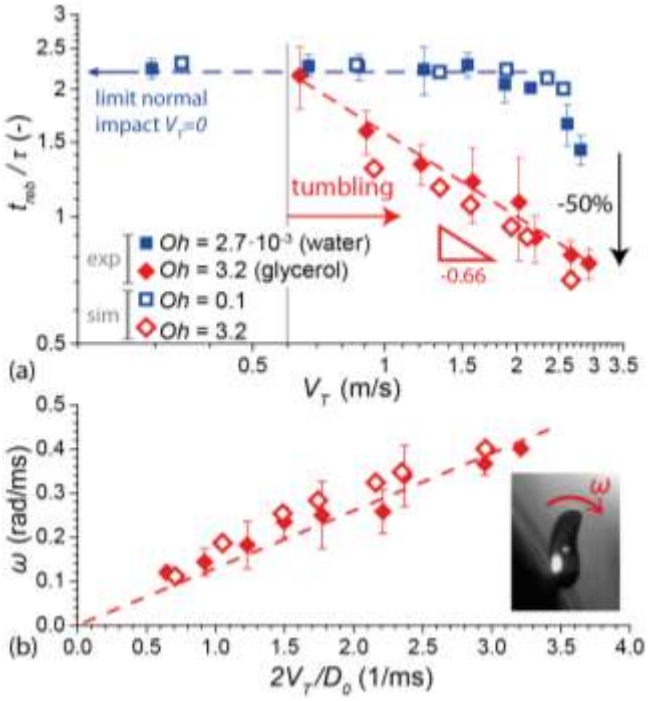

Figure 4: (a) The non-dimensional rebound time, t_{reb}/τ, as function of the tangential velocity, V_T: both experimental data for water and glycerol and numerical results are included. Legend reports values of Oh. (b) The angular velocity, ω, of highly viscous glycerol drop scales linearly with $2V_T/D_0$. Solid symbols: experiments; open symbols: simulations. The fitting line is $\omega = 0.13\left(2V_T/D_0\right)$.

Figure 4a shows the variation of the rebound time as function of the tangential velocity for water and glycerol. Unsurprisingly, for water ($Oh = 2.7\cdot10^{-3}$), the rebound time remains constant for a wide range of tangential impact velocity, up to $V_T \approx 2\,\mathrm{m/s}$, and $t_{reb}/\tau = 2.2$ still holds, meaning that the spreading and recoiling process of the drop is not affected by the simultaneous downward sliding. In other words, the usual picture of the inertia-capillarity interplay during the conventional rebound still holds and the viscosity (if low) does not play a prominent role. Only for $V_T > 2\,\mathrm{m/s}$, the impact deviates from the classical axisymmetric behavior: as demonstrated recently by Bird *et al.* [20] in the context of engineered superhydrophobic surfaces, the non-axisymmetric spreading and recoiling (see Video 7 in the Supplemental Material) can lead to a reduction of drop rebound time down to $t_{reb}/\tau \approx 1.5$ for the maximum tested tangential velocity

($V_T \approx 3\,\mathrm{m/s}$). A comparison of the drop shape evolution resulting from ELBM simulations between the low-viscosity regime ($Oh = 0.1$, see Figure 5a and corresponding Video 8 in the Supplemental Material) and the high-viscosity regime ($Oh = 3.2$), highlights the same trend and confirms the limited role of viscosity on drop dynamics in the regime $Oh < 1$.

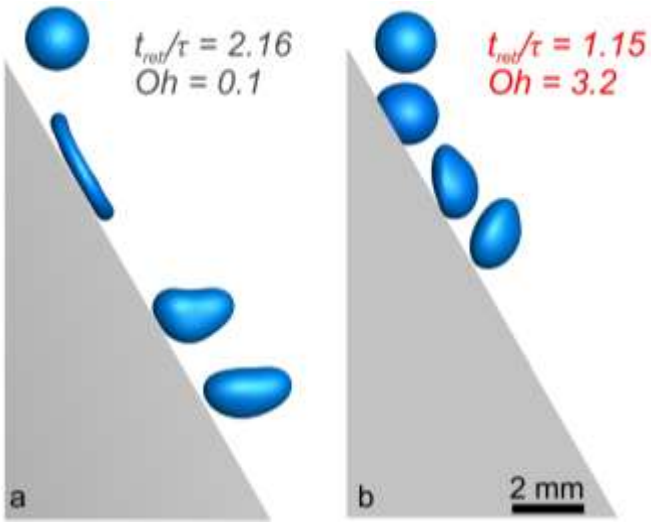

Figure 5: Evolution of simulated drop impacting on a sublimating slope: (a) a drop in the low viscosity regime ($Oh = 0.1$, $We = 121$, $\alpha = 60^\circ$), and (b) a drop in the high viscosity regime ($Oh = 3.2$, $We = 121$, $\alpha = 60^\circ$). The rebound time in the simulation was identified through matching the experimentally observed orientation of the drop at the rebound with the corresponding simulated image.

However, for highly viscous glycerol drops ($Oh = 3.2$) a fundamentally different rebound mechanism is identified, as highlighted previously in Figure 1c. The drop rebound starts at $V_T \approx 0.6\,\mathrm{m/s}$ with a rebound time of $t_{reb}/\tau \approx 2.2$ (see Figure 4a), similar to that of water at the same V_T, and is significantly reduces down to a minimum of $t_{reb}/\tau \approx 0.7$ at the highest tested tangential velocity, $V_T = 3\,\mathrm{m/s}$. The glycerol rebound time is thus half that of water above $V_T = 3\,\mathrm{m/s}$, despite the fact that glycerol drops do not rebound for $V_T < 0.6\,\mathrm{m/s}$ and even with the three orders of magnitude higher viscosity of glycerol compared to water (Figure 4a).

199 The reason for faster rebound at high viscosity is that, after some spreading and limited sliding, the drop
200 tumbles off without recoiling. The drop rapidly detaches from the surface by rotating almost as a rigid
201 body. The transition to a different rebound regime at high viscosities can be understood by comparing the
202 drop relaxation time, $t_{rel} \propto \mu D_0 / 2\sigma$ [42], to the characteristic oscillation time, τ, whose ratio is
203 proportional to Oh. Indeed, at high viscosities, when $t_{rel} / \tau \sim Oh > 1$, the longer t_{rel} delays drop recoiling
204 and leads to sustaining the drop rotational energy during tumbling. Also, the distance travelled by the drop
205 through sliding, $L_{slide} = V_{slide} t_{reb}$, is significantly reduced for high Oh, since both V_{slide} and t_{reb} are
206 reduced with increasing Oh, as shown in Figure 3 and Figure 4, respectively. Figure 4b shows that the
207 average drop angular (spinning) velocity, ω, scales linearly with the ratio $2V_T / D_0$ (see section SM5 in the
208 Supplemental Material for more details). The average angular velocity, ω, was defined and measured as
209 the ratio of the angle formed by the major axis of the flattened drop and the substrate at the moment of
210 drop lift-off (Ω_{reb}), and the rebound time, t_{reb}. Indeed, since the balance of the drop angular momentum
211 gives $F_{fr} D_0 / 2t_{fr} \approx I\omega / t_{fr}$, on the basis of the above estimation for F_{fr} we obtain $\omega \approx (1-k)(2V_T / D_0)$,
212 confirming the linear correlation. Figure 6 shows the value of Ω_{reb} as function of the impact tangential
213 velocity, V_T: Ω_{reb} is practically constant in the range ~60-70° for $V_T > 1.3\,\mathrm{m/s}$. As such, an increase of
214 angular velocity, ω, corresponding to a faster spinning, is responsible for a significant reduction of the
215 rebound time, t_{reb}, for very viscous liquids with $Oh > 1$ (glycerol, $Oh = 3.2$), compared to the three orders
216 of magnitude less viscous water.

217

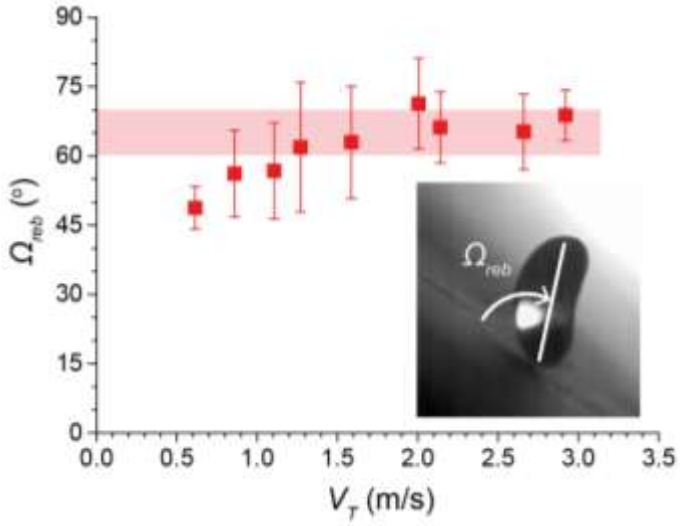

Figure 6: Values of the drop tilting angle at the moment of rebound, Ω_{reb}, as function of tangential component of velocity, V_T, for a highly viscous glycerol drop (Oh=3.2).

The occurrence of tumbling can be better understood within the framework of vorticity generation from a boundary (shear) layer. Injection of vorticity through a shear layer was studied, in particular by [43] in a direct numerical simulation of a drop normal impact onto a flat surface. Transition to tumbling under shear is a common scenario also away from boundaries [44]. In the present experiment, the tilted slope provides an off-center impact condition and thus can cause generation of the angular momentum. Hence, when a viscous drop impacts on the sublimating surface, the linear momentum of the drop is partially converted into angular momentum, providing the drop with a spin that facilitates take off causing tumbling. Note that the energy associated with the rotation, $R \sim mD_0^2\omega^2/8$ is small compared to the tangential component of translational kinetic energy $K \sim mV_T^2/2$. Since $\omega = 0.13\left(2V_T/D_0\right)$ (Figure 4b), then $R/K \sim 10^{-2}$; that is, only about one percent of the drop initial kinetic energy is converted into rotational energy.

C Vorticity generation and evolution

To better identify the origin of the tumbling effect, the local angular velocity was calculated from the numerical simulations as $\vec{\omega}_{loc} = \left|\vec{r} \times \vec{v}\right| / r^2$, where $\vec{r}$ is the position vector relative to the center-of-mass of

the drop, and $\vec{v}$ is the relative fluid velocity at that location. The component of the vector $\vec{\omega}_{loc}$, orthogonal to the plane of symmetry of the impacting drop, is overwhelmingly dominant, i.e. two orders of magnitude larger than the other two orthogonal components, since the rotation axis is essentially perpendicular to the plane of symmetry. From this dominant component, the average instantaneous angular velocity over the drop volume, $\omega(t)$, was computed: its evolution is illustrated in Figure 7 (see also corresponding Video 9), together with the characteristic snapshots of the local angular velocity spatial distribution on the symmetry plane; ω rapidly reaches a maximum value well before rebounding, with the rotational motion initiated near the impact zone and then becoming uniform. Thereafter, ω remains practically constant through the liquid, with the drop exhibiting the behavior of a solid ready to tumble. Put differently, the oblique impact breaks the axisymmetry of the drop at the beginning of the sliding, and the gain in angular momentum is thus initiated by the off-center flow reversal. If the relaxation time is large enough ($Oh > 1$), the angular momentum diffuses through the entire drop before it can recoil, and the tumbling takes place.

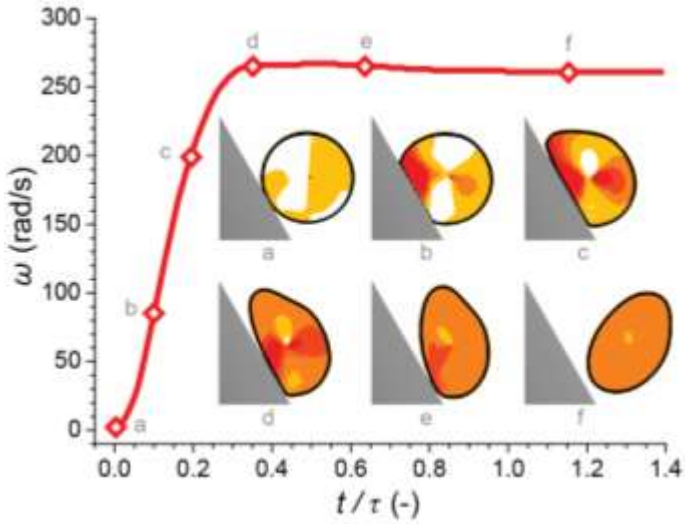

Figure 7: History of the average angular velocity, ω, of highly viscous liquid drop with $Oh = 3.2$, $We = 121$, $\alpha = 60^{\circ}$ during tumbling (simulation). Propagation of the dominant angular velocity component of $\vec{\omega}_{loc}$ inside the drop is shown in the insets (a-f), at different stages of tumbling. Stages a-c: Initial rise of the angular velocity shortly after the impact; Stages d-f: Rotation of the drop acting essentially as a solid. Drop rebounds (f) at $t/\tau = 1.15$. Shading/color increase corresponds to the increase of the clock-wise rotation.

For comparison, Figure 8 shows the history of the averaged angular velocity, ω, in the low viscosity regime ($Oh = 0.1$), together with the characteristic snapshots of the distribution of the local angular velocity during impact (see also Video 10). Unlike in the case of high viscosity, the angular velocity gained initially in the impact (phase a-c in Figure 8) is not sustained at a constant value during the extension and sliding (phase c-d), and no solid-like tumbling is observed. At the final stage close to the rebound (f), a small gain of the average angular velocity is due to the merging of the dumbbell-like shape of the drop at the intermediate stage, with non-axisymmetric collapse of the rim from (d) to (e). In other words, in the low viscosity regime the fluid slips away and the rotation is not sustained.

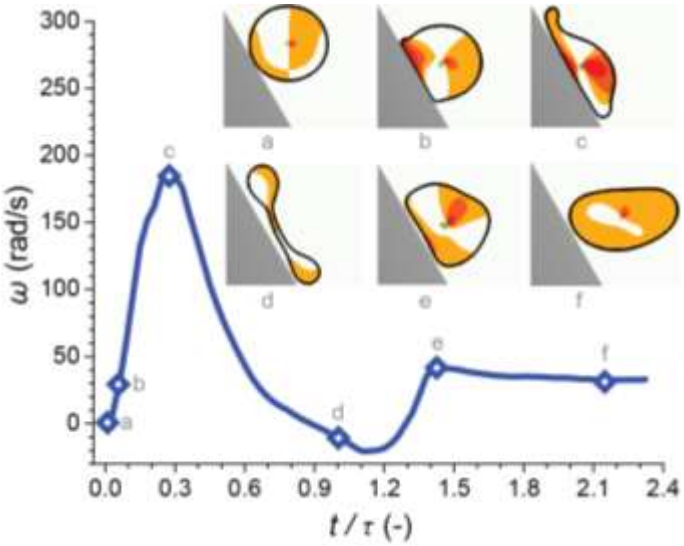

Figure 8: History of the average angular velocity ω of low viscosity liquid drop with $Oh = 0.1$, $We = 121$, and slope $\alpha = 60^{\circ}$ (simulation). Propagation of the dominant angular velocity component of $\vec{\omega}_{loc}$ inside the drop is shown in the insets (a-f), at different stages of drop impact. Drop rebounds (f) at $t/\tau = 2.1$. Shading/color increase corresponds to the increase of the clock-wise rotation.

IV CONCLUSIONS

Taken together, our results demonstrate and explain the existence of a new, prompt tumbling-rebound regime for non-axisymmetric drop impact on surfaces under slip conditions, here readily realized with the help of a sublimating slope. To this end, sublimating surfaces present themselves as an interesting, easy to use platform for the study of unexplored, liquid-surface interactions, especially in the limit of small friction,

brought about by the absence of direct contact between the liquid and the solid surface. Similar effects could be possible also on superhydrophobic surfaces, if they are fabricated to reach extreme performance. Preliminary simulations for contact angles $170^o < \theta < 180^o$ indicate that tumbling-rebound could take place, opening an interesting direction of future work, e.g. to promote repellence of viscous supercooled drops in icing conditions [30,45].

V Acknowledgments

CA acknowledges funding through a Marie Curie Intra-European Fellowship (ICE^2, 301174). IK and SC were supported by the ERC grant 291094-ELBM. AM was supported by the ETH grant ETH35-12-2. Computational resources at CSCS, Switzerland, were provided under the grant S492. The authors acknowledge Marti Ueli (ETH Zurich) for technical support in the liquid viscosity measurement.

VI References

[1] I. V. Roisman, E. Berberović, and C. Tropea, Phys. Fluids **21**, 052103 (2009).

[2] I. V. Roisman, Phys. Fluids **21**, 052104 (2009).

[3] A. L. Yarin, Annu. Rev. Fluid Mech. **38**, 159 (2006).

[4] M. Marengo, C. Antonini, I. V. Roisman, and C. Tropea, Curr. Opin. Colloid Interface Sci. **16**, 292 (2011).

[5] D. Bonn, J. Eggers, J. Indekeu, J. Meunier, and E. Rolley, Rev. Mod. Phys. **81**, 739 (2009).

[6] M. Mani, S. Mandre, and M. P. Brenner, J. Fluid Mech. **647**, 163 (2010).

[7] S. Mandre and M. P. Brenner, J. Fluid Mech. **690**, 148 (2011).

[8] G. Riboux and J. M. Gordillo, Phys. Rev. Lett. **113**, 024507 (2014).

[9] L. Xu, Phys. Rev. E **75**, 056316 (2007).

[10] L. Xu, W. Zhang, and S. Nagel, Phys. Rev. Lett. **94**, 184505 (2005).

[11] C. Antonini, I. Bernagozzi, S. Jung, D. Poulikakos, and M. Marengo, Phys. Rev. Lett. **111**, 014501 (2013).

[12] L. H. J. Wachters and N. A. J. Westerling, Chem. Eng. Sci. **21**, 1047 (1966).

[13] A. L. Biance, C. Clanet, and D. Quéré, Phys. Fluids **15**, 1632 (2003).

[14] T. Tran, H. J. J. Staat, A. Prosperetti, C. Sun, and D. Lohse, Phys. Rev. Lett. **108**, 036101 (2012).

[15] T. Tran, H. J. J. Staat, A. Susarrey-Arce, T. C. Foertsch, A. van Houselt, H. J. G. E. Gardeniers, A. Prosperetti, D. Lohse, and C. Sun, Soft Matter **9**, 3272 (2013).

[16] J. M. Kolinski, S. M. Rubinstein, S. Mandre, M. P. Brenner, D. A. Weitz, and L. Mahadevan, Phys. Rev. Lett. **108**, 074503 (2012).

[17] J. M. Kolinski, L. Mahadevan, and S. M. Rubinstein, Phys. Rev. Lett. **112**, 134501 (2014).

[18] J. de Ruiter, R. Lagraauw, D. van den Ende, and F. Mugele, Nat. Phys. **adv online**, (2014).

[19] D. Richard, C. Clanet, and D. Quéré, Nature **417**, 811 (2002).

[20] J. C. Bird, R. Dhiman, H.-M. Kwon, and K. K. Varanasi, Nature **503**, 385 (2013).

[21] Y. Liu, L. Moevius, X. Xu, T. Qian, J. M. Yeomans, and Z. Wang, Nat. Phys. **10**, 515 (2014).

[22] C. Antonini, F. Villa, I. Bernagozzi, A. Amirfazli, and M. Marengo, Langmuir **29**, 16045 (2013).

[23] M. A. Goldshtik, V. M. Khanin, and V. G. Ligai, J. Fluid Mech. **166**, 1 (2006).

[24] J. Snoeijer, P. Brunet, and J. Eggers, Phys. Rev. E **79**, 036307 (2009).

[25] P. Brunet and J. H. Snoeijer, Eur. Phys. J. Spec. Top. **192**, 207 (2011).

[26] G. Lagubeau, M. Le Merrer, C. Clanet, and D. Quéré, Nat. Phys. **7**, 395 (2011).

[27] D. Quéré, Annu. Rev. Fluid Mech. **45**, 197 (2013).

[28] I. U. Vakarelski, N. A. Patankar, J. O. Marston, D. Y. C. Chan, and S. T. Thoroddsen, Nature **489**, 274 (2012).

[29] H.-J. Butt, C. Semprebon, P. Papadopoulos, D. Vollmer, M. Brinkmann, and M. Ciccotti, Soft Matter **9**, 418 (2013).

[30] T. Maitra, C. Antonini, M. K. Tiwari, A. Mularczyk, Z. Imeri, P. Schoch, and D. Poulikakos, Langmuir **30**, 10855 (2014).

[31] R. Rioboo, M. Voué, a Vaillant, and J. De Coninck, Langmuir **24**, 14074 (2008).

[32] L. F. Loucks, J. Chem. Educ. **63**, 115 (1986).

[33] A. Mazloomi, S. S. Chikatamarla, and I. V. Karlin, Phys. Rev. Lett. **114**, 174502 (2015).

[34] I. V. Karlin, A. N. Gorban, S. Succi, and V. Boffi, Phys. Rev. Lett. **81**, 6 (1998).

[35] S. S. Chikatamarla, S. Ansumali, and I. V. Karlin, Phys. Rev. Lett. **97**, 010201 (2006).

[36] S. S. Chikatamarla and I. V. Karlin, Phys. Rev. Lett. **97**, 190601 (2006).

[37] J. Zhang and D. Y. Kwok, Langmuir **20**, 8137 (2004).

[38] A. Mazloomi M., S. S. Chikatamarla, and I. V. Karlin, Phys. Rev. E **92**, 023308 (2015).

[39] E. Pierce, F. J. Carmona, and A. Amirfazli, Colloids Surfaces A Physicochem. Eng. Asp. **323**, 73 (2008).

[40] H. B. Eral, D. J. C. M. 't Mannetje, and J. M. Oh, Colloid Polym. Sci. **291**, 247 (2012).

[41] C. Antonini, F. Villa, and M. Marengo, Exp. Fluids **55**, 1713 (2014).

[42] K. Moran, A. Yeung, and J. Masliyah, J. Colloid Interface Sci. **267**, 483 (2003).

[43] R. D. Schroll, C. Josserand, S. Zaleski, and W. W. Zhang, Phys. Rev. Lett. **104**, 034504 (2010).

[44] J. M. Skotheim and T. W. Secomb, Phys. Rev. Lett. **98**, 078301 (2007).

[45] T. M. Schutzius, S. Jung, T. Maitra, P. Eberle, C. Antonini, C. Stamatopoulos, and D. Poulikakos, Langmuir **31**, 4807 (2015).